

Cyclotron orbit knot and tunable-field quantum Hall effect

Yi Zhang^{1, 2, 3, 4}

¹*International Center for Quantum Materials, Peking University, Beijing, 100871, China*

²*School of Physics, Peking University, Beijing, 100871, China*

³*Department of Physics, Cornell University, Ithaca, NY 14853, USA*

⁴*Kavli Institute for Theoretical Physics, University of California, Santa Barbara, CA 93106, USA*

From a semi-classical perspective, the Bohn-Sommerfield quantization of the closed cyclotron orbits for charged particles such as electrons in an external magnetic field gives rise to discrete Landau levels and a series of fascinating quantum Hall phenomena. Here, we consider topologically nontrivial physics from a distinct origin, where the cyclotron orbits take nontrivial knotting structures such as a trefoil knot. We present a scenario of an unconventional Weyl semimetal with a slab geometry, where the Fermi arcs on the opposing surfaces can cross without interfering with each other and form a knot together with the bulk Weyl nodes, and in an external magnetic field, the resulting chiral Landau levels. We provide a microscopic lattice model to realize a cyclotron orbit with a geometry of a trefoil knot and study the corresponding quantum oscillations. Interestingly, unlike the conventional ring-shaped cyclotron orbit, a trefoil knot is self-threading, allowing the magnetic field line along the novel cyclotron orbit to contribute to the overall Berry phase, therefore altering the external magnetic field for each quantization level. The cyclotron orbit knot offers a new arena of the nontrivial knot theory in three spatial dimensions and its subsequent physical consequences.

Integer quantum Hall effect¹ and the subsequently-discovered zoo of miscellaneous topological phases^{2–10} represent an active research area in condensed matter physics. The physics idea, however, may trace back further to the insightful semiclassical quantization of the cyclotron orbits^{11,12}. Following the semiclassical equations of motion, charged particles such as electrons cycle in the plane normal to the magnetic field around the constant energy contours, which then become quantized according to the Bohn-Sommerfield quantization condition. In two dimensions, all electron degrees of freedom are quenched into these cyclotron orbits with discrete and degenerate energy values - the Landau levels - in a magnetic field. The spacing and degeneracy of the Landau levels are proportional to the magnetic field strength, giving rise to the oscillations in material electronic properties as a function of the applied magnetic field such as De Haasvan Alphen effect, Shubnikovde Haas effect and other fascinating facets of the quantum Hall effect.

A relatively young sibling in the topological material family is the topological Weyl and Dirac semimetals in three dimensions^{9,10}. Around the Weyl nodes - selected points in their Brillouin zone, the low-energy electronic excitations disperse linearly, resembling the Weyl fermions in models for high energy physics. Also, the surface electronic states consist of exotic open Fermi arcs^{9,10}. In the presence of a magnetic field, the Weyl fermions become quantized as the chiral Landau levels that disperse along or against the magnetic field depending on the Weyl fermions' chirality, exhibiting the chiral anomaly phenomenon¹³. These chiral Landau levels, together with the Fermi arcs on the top and bottom surface in a slab geometry, assemble a novel type of cyclotron orbits in the Dirac and Weyl semimetals, dubbed as the Weyl orbit^{14,15}, see Fig. 1(a) for illustration. The Weyl orbit extends in and promotes the Landau quantization to three spatial dimensions, and the corresponding quan-

tum oscillations¹⁶ and quantum Hall transports^{17–19} have been established experimentally.

The search for topological phenomena in condensed matter physics^{8,20} has received much inspiration from the mathematical studies on topology such as knot theory, which investigates the nonequivalent classes of closed loops and the corresponding invariants, e.g., the Jones polynomial, in higher dimensional spaces. Indeed, a series of two-dimensional topological orders are characterized by topological quantum field theory on nontrivial quasi-particle world-line knots in 2+1-dimensional space-time²⁰. Also, the topologically distinct fermionic excitations in the form of connected links and knots in momentum space are discovered in nodal link²¹ and nodal knot²² metals. In this work, we present our discovery of a new topology origin of quantum materials and phenomena, where the cyclotron orbit employs a nontrivial knot topology, such as a trefoil knot (Fig. 1(c)), in three spatial dimensions. Commonly, a cyclotron orbit is self-evading, since the couplings between nearby Fermi surfaces generally widen the gap and move them further apart, especially in a magnetic field, making crossings - a key ingredient of knots - difficult to realize. The Weyl orbits in the Dirac and Weyl semimetal slabs offer a solution to this difficulty, as the Fermi arcs on the top and bottom surfaces are spatially separated and can form crossings without interfering with each other. We provide a microscopic lattice model example where we realize a Weyl orbit with a trefoil knot geometry, see Fig. 1(b) and (d). In three spatial dimensions²³, such a cyclotron orbit knot is not adiabatically connected to a conventional ring-shaped cyclotron orbit including the conventional Weyl orbit in Fig. 1(a). In comparison, the nodal link²¹ and nodal knot²² metals rest their topological distinctions on the nodal line topology in three-dimensional momentum space. They remain gapless in the presence of a magnetic field and disperse in the momentum space

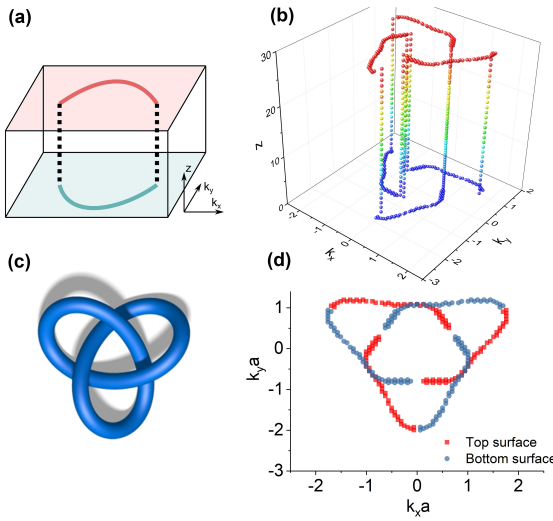


FIG. 1. (a) The Weyl orbit consists of the Fermi arcs on the top (red) and bottom (blue) surfaces and the chiral Landau levels from the Weyl nodes in the bulk (black dashed lines). This Weyl orbit is still topologically equivalent to a conventional ring-shaped cyclotron orbit. (b) The Fermi arcs of the Weyl semimetal model in Eq. 1 on the top and bottom surfaces of a slab and the bulk tunneling at the six Weyl nodes assemble a cyclotron orbit with a trefoil-knot geometry. For a better visibility, the points show the values of (k_x, k_y, z) for low-energy states within an energy window $E \in [-0.1, 0.1]$ around the Weyl nodes. In the presence of a magnetic field along \hat{z} , the shape of the cyclotron orbit in three spatial dimensions is related by a 90-degree rotation in the xy plane. (c) A trefoil knot is a closed loop with three crossings and topologically distinctive from a ring-shaped loop. (d) The projection of (b) onto the k_x, k_y plane demonstrates the three similar crossings to (c). Thanks to the spatial separation between the surfaces, the Fermi arcs manage to cross without interfering with each other.

along the magnetic field. Therefore, their nodal links and knots do not translate to their cyclotron orbits in three spatial dimensions.

The nontrivial topology of the cyclotron orbit knot also has profound physical consequences. For instance, unlike a ring-shaped loop, a knot is self-threading. Therefore a magnetic field line along a cyclotron orbit knot contributes nontrivially to the overall Berry phase around the orbit. Tuning this flux allows the contribution from other sources such as the magnetic field to differ in order to reach a specific Landau quantization. Using our microscopic lattice model, we study the behavior of the quantum oscillations associated with the cyclotron orbit knot. In particular, we introduce a perturbation that creates an effective magnetic field that aligns with the electronic velocity and study its impact on the subsequent quantum Hall effect.

Without loss of generality, we consider an electronic tight-binding model on a three-dimensional hexagonal

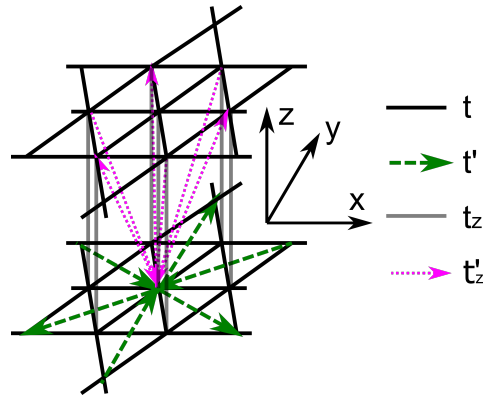


FIG. 2. Our local Hamiltonian in Eq. 1 describes a tight-binding model on the hexagonal lattice with four types of near-neighbor hoppings. The arrows denote imaginary amplitudes where the phase is i for hoppings along the arrow and $-i$ against the arrow. All lattice constants are set to $a = c = 1$.

lattice for concreteness:

$$\begin{aligned}
 H = & \sum_{\langle ij \rangle, z, s} t (-1)^z c_{jzs}^\dagger c_{izs} + \sum_{\langle\langle ik \rangle\rangle, z, s} t'_{ik} (-1)^z \sigma_{ss}^z c_{kzs}^\dagger c_{izs} \\
 & + \sum_{i, \langle zz' \rangle, s} t_z \sigma_{ss}^z c_{iz's}^\dagger c_{izs} + \sum_{\langle ij \rangle, \langle zz' \rangle, s} t''_{izjz'} (-1)^z c_{jz's}^\dagger c_{izs} \\
 & + \sum_{i, z' = z+1, s, s'} i \Delta \sigma_{ss'}^x (c_{iz's'}^\dagger c_{izs} - c_{izs}^\dagger c_{iz's'}) \\
 & - \sum_{i, z, s} \mu_s (-1)^z c_{izs}^\dagger c_{izs}
 \end{aligned} \quad (1)$$

where i, j, k are the coordinates in the xy plane and σ are the Pauli matrices defined on the two pseudo-spins²⁴ $s, s' = \uparrow, \downarrow$. The first two terms are hoppings in the xy plane between the nearest neighbors and the next nearest neighbors, $t'_{ik} = \pm i t'$ and the \pm sign depends on whether the direction from site i to k is along or against the arrow in Fig. 2. The next two terms are near-neighbor hoppings between the nearest layers, $t''_{izjz'} = \pm i t'_z$ and the sign \pm depends on the direction from site i, z to j, z' , see Fig. 2. The last two terms are a coupling between the two pseudo-spins $s, s' = \uparrow, \downarrow$ and a chemical potential. In the rest of the paper, we set $t = -1.0$, $t' = -0.5$, $t_z = -1.0$, $t'_z = -0.5$, $\Delta = 0.4$, $\mu_\uparrow = -5.1$, and $\mu_\downarrow = -3.5$ unless noted otherwise.

First of all, this model system is a Weyl semimetal. To see this, we transform Eq. 1 into the momentum space $H = \sum_{\mathbf{k}} H_{\mathbf{k}}$, with

$$\begin{aligned}
 H_{\mathbf{k}} = & \tau^z [\epsilon_0(k_\perp) + \sigma^z \epsilon_z(k_\perp)] + \tau^x \sigma^z 2 t_z \cos k_z \\
 & + \tau^y 4 t'_z \sin k_z (\sin k_1 + \sin k_2 + \sin k_3) - \tau^x \sigma^x 2 \Delta \sin k_z
 \end{aligned} \quad (2)$$

where τ are the Pauli matrices on the even-odd layers. $k_z \in [0, \pi]$ is the momentum along the \hat{z} direction, and $k_1 = k_x$, $k_2 = (-k_x + \sqrt{3}k_y)/2$, $k_3 = (-k_x - \sqrt{3}k_y)/2$ are momenta in the xy plane. $\epsilon_0(k_\perp) + \sigma^z \epsilon_z(k_\perp)$ are the Fourier transform of the t , t' and μ_s terms. There

are six Weyl nodes on the $k_z = \pi/2$ plane at $(k_x, k_y) = (0, -1.96)$ with $\sigma_z \simeq \uparrow$ and $(k_x, k_y) = (0, -0.834)$ with $\sigma_z \simeq \downarrow$ and their counterparts after the C_3 rotations²⁵. The band gap closes at these Weyl nodes, and the low-energy dispersion around them is linear. Interestingly, for a model system with a finite thickness L_z along the \hat{z} direction, the surface Fermi arcs consist of three Fermi arcs on the top surface and three on the bottom surface. The (k_x, k_y, z) location of the Fermi arcs and the bulk states at the Weyl nodes are shown in Fig. 1(b) for $L_z = 29$, thick enough to separate the Fermi arc states on the opposing surfaces. Therefore, the constant energy contour employs a trefoil knot [Fig. 1(c)]. In addition, we can no longer separate the six Weyl nodes into isolated pairs following the surface Fermi arc connectivity, as the contour engages all of the six Weyl nodes at once in this unconventional Weyl semimetal.

In the presence of an applied magnetic field along \hat{z} , the electrons cycle around the cyclotron orbit, whose shape in three spatial dimensions is related by a 90-degree rotation in the xy plane. Therefore, we have established a cyclotron orbit with a trefoil knot geometry that is topologically distinctive and not adiabatically connected with the conventional ring-shaped cyclotron orbits. We note the important role the Weyl orbit physics plays in attaining cyclotron orbit knots: the top and bottom Fermi arcs are spatially separated and can safely traverse each other without being gapped out even in the presence of a variable magnetic field. Together with the bulk chiral Landau levels that descend from the Weyl nodes and weave the two surfaces back together, we can form crossings that are the cornerstones for knots and links. The construction of trefoil-knot-shaped cyclotron orbit can be straightforwardly generalized to cyclotron orbits with more complex knots and links.

Next, we study the Landau quantization of the cyclotron orbit knot and consider the Hamiltonian in Eq. 1 with a slab thickness of $L_z = 29$ in the presence of a magnetic vector potential $\vec{A} = (-By, 0)$. Physical quantities such as the density of states (DOS) at the energy of the Weyl nodes can be obtained using the recursive Green's function method for sufficiently large system sizes. The results on the DOS versus the inverse magnetic field are summarized in Fig. 3. We observe a single quantum oscillation period of $\Delta(1/B) = 1/B_{n+1} - 1/B_n \simeq 4.87$. Since the bulk chiral Landau levels are parallel to the magnetic field, the quantum oscillations of a Weyl orbit is determined by the area S_k of the combined Fermi arcs from the top and bottom surfaces¹⁵. Interestingly, after projection and combination of the Fermi arcs [Fig. 1(d)], the area within the inner contour is $S_{k2} \sim 4.78\% \times S_{BZ}$ of the surface Brillouin zone area S_{BZ} , and the area within the outer contour (including S_{k2}) is $S_{k1} \sim 15.2\% \times S_{BZ}$. That $\Delta(1/B) \simeq (S_{k1} + S_{k2})^{-1} = 5.0$ indicates the magnetic flux enclosed in the inner contour contributes to the overall Berry phase twice. Indeed, straightforward counting suggests that the cyclotron orbit encloses the inner region twice upon each cycle. More rigorously, the con-

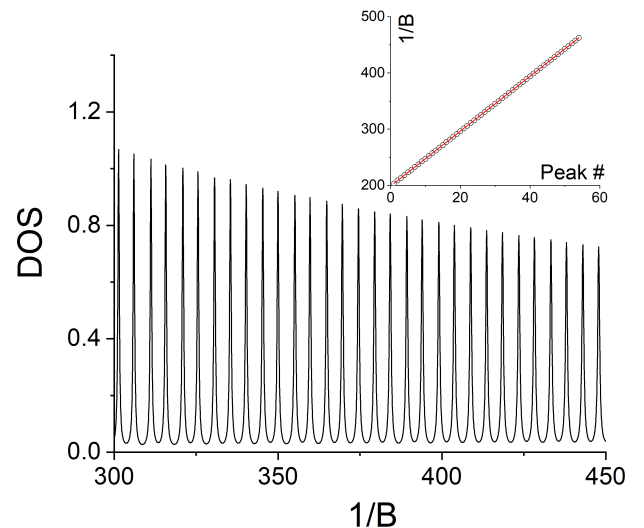


FIG. 3. The DOS versus the inverse magnetic field $1/B$ shows clear quantum oscillations with a single period. The Hamiltonian in Eq. 1 with a magnetic vector potential $\vec{A} = (-By, 0)$ is calculated using the recursive Green's function method. We focus on the chemical potential at the Weyl nodes and consider a slab with thickness $L_z = 29$. A small imaginary part $\delta = 0.001$ is added to the energy to account for a finite level width. Inset: a linear fit to the peak position within the $200 < 1/B < 500$ range reveals a quantum oscillation period of $\Delta(1/B) \simeq 4.87$.

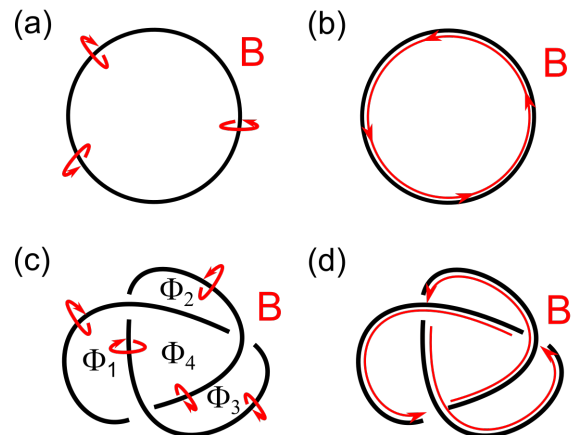


FIG. 4. The magnetic field line \mathbf{B} (red arrows) for ring-shaped and trefoil-knot-shaped cyclotron orbits. (a) A magnetic field line through the ring contributes a Berry phase. (b) The magnetic field line along the ring-shaped cyclotron orbit has no Berry phase contribution. (c) The magnetic field line through the trefoil knot contributes a Berry phase. The contributions from the fluxes in different regions $\Phi_{total} = \sum_{i=1}^4 \alpha_i \Phi_i$ obey $\alpha_1 = \alpha_2 = \alpha_3 = \alpha_4/2$. (d) Since a trefoil knot winds around itself, the magnetic field line along the cyclotron orbit knot now contributes a non-zero Berry phase.

tributions to the overall Berry phase $\Phi_{total} = \sum_{i=1}^4 \alpha_i \Phi_i$ obeys $\alpha_1 = \alpha_2 = \alpha_3 = \alpha_4/2$, since the adiabatic change as illustrated in Fig. 4(c) of a magnetic field loop with flux Φ indicates the equivalence $\alpha_1 \Phi = \alpha_2 \Phi = \alpha_3 \Phi = (\alpha_4 - \alpha_1) \Phi = (\alpha_4 - \alpha_3) \Phi$. On that account, our numerical results on quantum oscillations are fully consistent with the trefoil knot geometry of the cyclotron orbit.

Then, we discuss an interesting physical consequence of the nontrivial knot geometry of a cyclotron orbit - the tunable-field quantum Hall effect. Conventionally, the magnetic field line along the ring-shaped cyclotron orbit does not contribute to the overall Berry phase [Fig. 4(b)]. In contrast, a trefoil knot is self-threading, and thus the magnetic field line along the cyclotron orbit knot contributes nontrivially to the overall Berry phase, see Fig. 4(d). By controlling the contribution from such flux, we can modify the Landau quantization condition for other sources of the Berry phase, such as the applied magnetic field. The conventional spin-orbit interaction introduces a \vec{v} -dependent effective magnetic field that couples to the electron spin; to observe the tunable-field quantum hall effect here, we need to introduce a \vec{v} -dependent effective magnetic field that couples to the electron orbital angular momentum.

In the case of a knotting Weyl orbit, since the Fermi arcs locally responsible for the crossings are on the surfaces, we limit our attention to the effective magnetic fields in the xy plane. For instance, along the \hat{y} direction, we may introduce a \vec{v} -dependent effective magnetic field with a perturbation $H' \propto v_y (\vec{k} + \eta z \hat{x}) - v_y (\vec{k} - \eta z \hat{x}) \simeq 2i\eta z [x, v_y]$ for small η , where $v_y = i[y, H]$ is the electron velocity in the \hat{y} direction. However, it leads to a $\sin(k_3) - \sin(k_2)$ azimuthal angle dependence and vanishes after taking into account the $-\frac{1}{2}\hat{y} \pm \frac{\sqrt{3}}{2}\hat{x}$ directions. Therefore, we introduce an additional factor of $\cos(k_1)$, which is ~ 1 and a good approximation near the Weyl nodes and the crossing point where v_y is the most important. After similar treatment to the $-\frac{1}{2}\hat{y} \pm \frac{\sqrt{3}}{2}\hat{x}$ directions, we obtain in total:

$$H' = \sum_{\langle\langle ik \rangle\rangle, z'=z+1, s} t'_z \exp(3i\phi_{ik}) c_{kz's}^\dagger c_{izs} \times \eta z (-1)^z + \text{h.c.} \quad (3)$$

where ϕ_{ik} is the azimuthal angle from i to k and characterizes an angle-dependent $\pm i$ phase. For slowly varying ηz , $H' = \sum_{\mathbf{k}} H'_{\mathbf{k}}$ takes a momentum-space form

$$H'_{\mathbf{k}} \simeq \tau^y 4t'_z \eta z \times \sin k_z [\sin(k_2 - k_1) + \sin(k_3 - k_2) + \sin(k_1 - k_3)] \quad (4)$$

that only has τ^y component and thus does not interfere with the quantum oscillation period, which is determined by the combined surface Fermi arcs¹⁵ and the τ^z terms in the original $H_{\mathbf{k}}$ in Eq. 3. However, H' does have an interesting impact on the model physics²⁶.

As we include the perturbation H' into the original Hamiltonian H in Eq. 1, the magnetic field

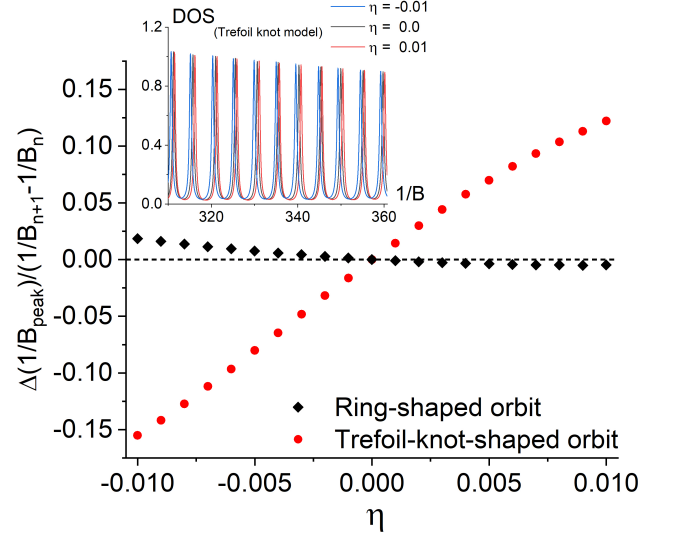


FIG. 5. The shifts of the DOS quantum oscillation peak positions $1/B_{\text{peak}}$ versus the amplitude η of the applied perturbation in Eq. 3. We track the DOS peak at $1/B \sim 227.78$ at $\eta = 0$ for the cyclotron orbit knot model and the DOS peak at $1/B \sim 223.61$ at $\eta = 0$ for the conventional Weyl orbit model as the $\sigma^z = \uparrow$ sector of $H + H'$ in Eq. 1 and 3. The perturbation creates an effective magnetic flux that contributes to the cyclotron orbit knots, and changes the Landau quantization condition for the magnetic field, see the red dots. In comparison, the $1/B$ quantization condition, shown as the black diamonds, hardly changes for the conventional ring-shaped Weyl orbit. Inset: the DOS peaks for the cyclotron orbit knot models displace with η yet retain an identical quantum oscillation period of $\Delta(1/B) \simeq 4.87$ for $\eta = 0, \pm 0.01$.

B corresponding to each Landau level changes. We track the shift of the DOS quantum oscillation peak $\Delta(1/B_{\text{peak}}) = 1/B_{\text{peak}}(\eta) - 1/B_{\text{peak}}(\eta = 0)$ as a function of η , and the results are summarized in Fig. 5. The ratio $\Delta(1/B_{\text{peak}}) / (1/B_{n+1} - 1/B_n)$ measures the Berry phase contributed by the perturbation in unit of the magnetic flux quantum. On the other hand, the period of the quantum oscillations remains unchanged, see Fig. 5 inset. Linear fits to 40 peak positions within the $200 < 1/B < 400$ range indicate an identical period of $\Delta(1/B) \simeq 4.87$ for $\eta = 0, \pm 0.01, \pm 0.02$. Therefore, the inclusion of H' induces an *extra yet constant* phase to the cyclotron orbit knot.

In fact, the tunable-field quantum Hall effect is not fully unheard of - the overall Berry phase of the Weyl orbit receives a contribution from the bulk chiral Landau levels that depends on the Fermi energy, the tilting direction of the applied magnetic field, as well as the thickness of the system^{15,19}. The extra Berry phase in this work, however, is consequential to the nontrivial knotting topology of the cyclotron orbit and comes from a completely different origin: with or without the H' perturbations, our model systems are still C_3 rotation

symmetric, the Fermi energy is at the Weyl nodes, and the magnetic field is along \hat{z} without tilting. Indeed, this contribution is unique to the cyclotron orbit knot model. In contrast, such an in-plane effective magnetic field incurs no orbital effect for conventional cyclotron orbits in two-dimensional electron systems. Further, we repeat the calculations for the $\sigma^z = \uparrow$ sector of the original Hamiltonian H in Eq. 1, which describes a conventional Weyl semimetal with a topologically-ring-shaped Weyl orbit. Its Weyl orbit also consists of three pairs of chiral Landau levels and three pieces of Fermi arcs on each of the top and bottom surfaces. As we change the amplitude η of the perturbation, given by the $\sigma^z = \uparrow$ sector of H' in Eq. 3, the DOS peaks in the quantum oscillations hardly shift, see the black diamond symbols in Fig. 5. The small deviations from ideal theory expectation may be due to the approximation in H' .

In conclusion, we have shown a new topological prospect where the cyclotron orbit takes a nontrivial knot geometry in three spatial dimensions and proposed the Weyl semimetal slab as an example of realization. We have also provided a microscopic lattice model, investigated its Landau quantization, and demonstrated that the unusual knotting topology of the cyclotron orbit allows the continuous tuning of the magnetic field condition for quantum Hall effect. We will study the realiza-

tion condition and transition of this unconventional Weyl semimetal, the Fermi arc properties on other surface directions, etc. in subsequent work.

Since the knots are topologically protected and invariant in three spatial dimensions, a cyclotron orbit knot is not adiabatically connected with the conventional ring-shaped cyclotron orbits and allowed to have characteristic topological properties. In topological quantum field theory, the nontrivial anyonic phases of quasi-particle braiding and statistics in two spatial dimensions are consequential to the nontrivial Jones polynomial of the knots between the quasi-particle world-lines in 2+1-dimensional space time²⁰. The consequences of cyclotron orbit knots in three spatial dimensions on characteristic properties, such as intrinsic Berry phase contributions, the scenarios beyond $U(1)$ gauge field, etc. and their connections to the knot invariants, are interesting further directions for future exploration.

Acknowledgment: YZ acknowledges support from the start-up grant at International Center for Quantum Materials, Peking University, the Bethe fellowship at Cornell University, and the National Science Foundation under Grant No. NSF PHY-1748958. The computation was supported by High-performance Computing Platform of Peking University.

¹ K. v. Klitzing, G. Dorda, and M. Pepper, Phys. Rev. Lett. **45**, 494 (1980).

² D. C. Tsui, H. L. Stormer, and A. C. Gossard, Phys. Rev. Lett. **48**, 1559 (1982).

³ R. B. Laughlin, Phys. Rev. Lett. **50**, 1395 (1983).

⁴ F. D. M. Haldane, Phys. Rev. Lett. **61**, 2015 (1988).

⁵ C. L. Kane and E. J. Mele, Phys. Rev. Lett. **95**, 146802 (2005).

⁶ L. Fu, C. L. Kane, and E. J. Mele, Phys. Rev. Lett. **98**, 106803 (2007).

⁷ M. Z. Hasan and C. L. Kane, Rev. Mod. Phys. **82**, 3045 (2010).

⁸ X. Chen, Z.-C. Gu, Z.-X. Liu, and X.-G. Wen, Science **338**, 1604 (2012).

⁹ X. Wan, A. M. Turner, A. Vishwanath, and S. Y. Savrasov, Phys. Rev. B **83**, 205101 (2011).

¹⁰ S.-Y. Xu, I. Belopolski, N. Alidoust, M. Neupane, G. Bian, C. Zhang, R. Sankar, G. Chang, Z. Yuan, C.-C. Lee, S.-M. Huang, H. Zheng, J. Ma, D. S. Sanchez, B. Wang, A. Bansil, F. Chou, P. P. Shibayev, H. Lin, S. Jia, and M. Z. Hasan, Science **349**, 613 (2015).

¹¹ L. Onsager, The London, Edinburgh, and Dublin Philosophical Magazine and Journal of Science **43**, 1006 (1952).

¹² I. Lifshitz and A. Kosevich, Journal of Experimental and Theoretical Physics **2**, 636 (1956).

¹³ H. Nielsen and M. Ninomiya, Physics Letters B **130**, 389 (1983).

¹⁴ A. C. Potter, I. Kimchi, and A. Vishwanath, Nature Communications **5** (2014), 10.1038/ncomms6161.

¹⁵ Y. Zhang, D. Bulmash, P. Hosur, A. C. Potter, and A. Vishwanath, Scientific Reports **6** (2016), 10.1038/srep23741.

¹⁶ P. J. W. Moll, N. L. Nair, T. Helm, A. C. Potter, I. Kimchi, A. Vishwanath, and J. G. Analytis, Nature **535**, 266 (2016).

¹⁷ C. Zhang, A. Narayan, S. Lu, J. Zhang, H. Zhang, Z. Ni, X. Yuan, Y. Liu, J.-H. Park, E. Zhang, W. Wang, S. Liu, L. Cheng, L. Pi, Z. Sheng, S. Sanvito, and F. Xiu, Nature Communications **8** (2017), 10.1038/s41467-017-01438-y.

¹⁸ C. M. Wang, H.-P. Sun, H.-Z. Lu, and X. C. Xie, Phys. Rev. Lett. **119**, 136806 (2017).

¹⁹ C. Zhang, Y. Zhang, X. Yuan, S. Lu, J. Zhang, A. Narayan, Y. Liu, H. Zhang, Z. Ni, R. Liu, E. S. Choi, A. Suslov, S. Sanvito, L. Pi, H.-Z. Lu, A. C. Potter, and F. Xiu, Nature **565**, 331 (2018).

²⁰ E. Witten, Communications in Mathematical Physics **121**, 351 (1989).

²¹ T. Bzdušek, Q. Wu, A. Rüegg, M. Sigrist, and A. A. Soluyanov, Nature **538**, 75 (2016).

²² R. Bi, Z. Yan, L. Lu, and Z. Wang, Phys. Rev. B **96**, 201305 (2017).

²³ The coordinates are momentum space in the xy plane and real space in \hat{z} . In a magnetic field along \hat{z} , the shape of the cyclotron orbit in three spatial dimensions is related by a 90-degree rotation in the xy plane.

²⁴ Other than resulting in different systematic symmetries, the model system and the conclusions also work for s and s' as the physical spins.

²⁵ The C_3 rotation symmetry is for simplicity and not a necessary ingredient of the cyclotron orbit knotting geometry.

²⁶ See Supplemental Materials for a perspective of H' as tilted chiral Landau levels¹⁵.